Mind the metal: a fragment library-derived zinc impurity binds the E2 ubiquitin-conjugating enzyme Ube2T and induces structural rearrangements

Francesca E. Morreale,[1] Andrea Testa,[2] Viduth K. Chaugule,[1] Alessio Bortoluzzi,[2] Alessio Ciulli,[2] Helen Walden,[1]**

[1] MRC Protein Phosphorylation and Ubiquitylation Unit, School of Life Sciences, University of Dundee, Dundee DD1 5EH, United Kingdom

[2] Division of Biological Chemistry and Drug Discovery, School of Life Sciences, University of Dundee, Dundee DD1 5EH, United Kingdom

KEYWORDS. Ubiquitin-conjugating enzymes, domain swap, false positives, metal-induced oligomerization, ubiquitination, X-ray crystallography

ABSTRACT

Efforts to develop inhibitors, activators and effectors of biological reactions using small molecule libraries are often hampered by interference compounds, artifacts and false positives that permeate the pool of initial hits. Here we report the discovery of a promising initial hit compound targeting the Fanconi anemia ubiquitin-conjugating enzyme Ube2T and describe its biophysical and biochemical characterization. Analysis of the co-crystal structure led to the identification of a contaminating zinc ion as solely responsible for the observed effects. Zinc binding to the active site cysteine induces a domain swap in Ube2T that leads to cyclic trimerization organized in an open ended linear assembly. Our study serves as a cautionary tale for screening small molecule libraries and provides insights into the structural plasticity of ubiquitin-conjugating enzymes.

INTRODUCTION

Many different mechanisms can lead to false positive signals when screening for small molecules binding to a protein of interest. Among them are compound aggregation, interference with the detection method, covalent and nonspecific crosslinking, redox reactions or presence of impurities.[1] Several molecules that yield false signals across different assays are known as PAINS (pan-assay interference compounds). Such compounds have defined structures and are repeatedly identified and published as promising hits against different proteins, however their activity does not depend on specific, drug-like interactions with the protein, and instead arise as the result of a variety of artifacts.[2] Some types of false positives are easier to detect and discard. For instance, using orthogonal assays is a common way to exclude interferences related to a particular detection method and using non-ionic detergents can effectively relieve enzyme inhibition by aggregated compounds.[3] In other cases, compound interference can be more difficult to recognize, especially when the observed effect is concentration dependent and consistent across different orthogonal assays.

We recently reported a fragment screening against the ubiquitin-conjugating enzyme Ube2T.[4] Ubiquitin-conjugating enzymes (E2s) possess a catalytic cysteine, which receives a ubiquitin molecule from the E1 (ubiquitin-activating enzyme) through a transthiolation reaction and, together with an E3 ligase, transfers it onto the lysine of a substrate. All E2s possess a core catalytic domain (~150 amino acids), known as UBC (ubiquitin-conjugating) fold that contains a conserved catalytic cysteine (Figure 1A). This domain is normally composed of four α helices and four β strands, occasionally enriched by insertion loops and N- or C-terminal extensions,

which are often intrinsically disordered.[5, 6] RING-type E3s facilitate ubiquitin transfer by binding the E2s on a surface that is distinct from the active site.[7, 8] This region comprises loops 1 and 2 and the first α helix of the UBC fold.

Ube2T shares the canonical UBC fold and presents a C-terminal extension (~ 40 residues), which is not visible in any of the published crystal structures.[4, 9, 10] Ube2T specifically interacts with the RING E3 ligase FANCL with a K_D of ~0.5 μM.[10, 11] This exclusive E2-E3 pair catalyzes the monoubiquitination of the heterodimeric FANCI/FANCD2 complex, which is the key signaling event to activate the Fanconi anemia pathway for DNA repair.[12, 13]

Here we report the detailed biophysical characterization and optimization attempts for what seemed to be the most promising hit compound of our fragment screening. The effects of this molecule were consistent and concentration dependent across a wide range of biophysical assays. Puzzlingly, most of the synthesized analogues resulted in complete loss of binding, even when modifications were minor. The crystal structure was crucial for explaining the lack of a consistent structure-activity relationship (SAR): the effects of our hit compound were solely due to a zinc contamination. Zinc induces an unprecedented arrangement in Ube2T by binding at two different sites on the protein: the first site mediates the formation of a domain swapped cyclic trimer, and the second site is responsible for the arrangement of the trimers in an open-ended linear assembly. Our study shows that the active site cysteine in Ube2T is susceptible to modification and reveals the plasticity of the E2 fold.

RESULTS AND DISCUSSION

Discovery of compound 1 as a potential Ube2T inhibitor

Compound **1** (Figure 1B) was identified as a hit in our recently published fragment screening against the ubiquitin-conjugating enzyme Ube2T.[4] The initial orthogonal screens using differential scanning fluorimetry (DSF) and bio-layer interferometry (BLI) both yielded compound **1** as a very promising hit showing a concentration dependent effect (Figure S1). Although compound **1** acted as a destabilizer in DSF, causing a decrease in Ube2T's melting temperature (even at low concentrations), we pursued this due to reports that destabilizing agents can be confirmed as true binders.[4, 14] In BLI, association and dissociation responses were observed also at the lowest concentration tested (2 μM), in contrast with other fragments which didn't show any binding at this concentration.

Having identified **1** as the most potent hit of our fragment screening, we were interested in characterizing it further and exploring its mechanism of action.

In order to map its binding site, we performed HSQC experiments using ^{15}N-labeled Ube2T$_{\Delta C}$ (residues 1-154, lacking the C-terminal flexible tail).[4] Upon addition of increasing compound **1** concentrations (100 μM, 300 μM and 500 μM), several resonance peaks became weaker and finally disappeared when an approximate 1:10 molar ratio was reached (500 μM **1**, Figure S2). Disappearance of the peaks suggested a tighter interaction of **1** compared to the other fragments tested, that only caused moderate shifts at millimolar concentrations. We confirmed that disappearance of the peaks was due to a genuine and reversible binding by dialyzing out compound **1** overnight. As expected, the signals' position in the free spectrum was restored after dialysis. These residues were mapped onto the available Ube2T crystal structures[4, 9, 10] and

appeared to be adjacent to the catalytic cysteine (Figure 1C). At this site however, no apparent pocket was present. We therefore speculated that a structural rearrangement needed to occur to accommodate a small molecule binding.

In order to obtain more insights into compound **1** binding, we performed isothermal titration calorimetry (ITC) experiments (Figure 1D and Table S1) and found that **1** binds Ube2T with a K_D = 17.7 μM (LE = 0.41 kcal mol^{-1}), a rather high affinity for a fragment.

In order to assess whether the binding of **1** was competitive with that of Ube2T cognate E3, we used a different construct in which Ube2T is fused to the RING domain of FANCL through a linker between the two proteins (Ube2T-$FANCL_{RING}$).[10] A similar K_D was obtained when **1** was titrated against the Ube2T-$FANCL_{RING}$ fusion protein (Figure 1D), confirming that **1** binds to a different site. In contrast, binding was completely lost when Ube2T carries a ubiquitin molecule at the active site (Ube2T-Ub, where ubiquitin is linked through an isopeptide bond to the C86K-K91R-K95R mutant Ube2T). This was consistent with the observation that the compound **1** binding site is adjacent to the catalytic cysteine (C86). We next investigated if **1** was able to affect Ube2T enzymatic activity using a biochemical assay. This assay monitors the first step of the ubiquitination cascade, which is the ability of Ube2T (the E2) to be ubiquitin-charged by the E1 on the catalytic cysteine via a transthiolation reaction. As shown in Figure 1E, in the absence of compound **1**, Ube2T is charged and autoubiquitinates itself as previously reported.[12] Addition of 100 μM **1** almost completely abolished Ube2T charging and this effect was concentration-dependent. In contrast, the same concentrations did not affect the E1-Ub charging in the absence of Ube2T (Figure 1E), indicating that **1** specifically inhibits Ube2T-Ub charging by the E1.

These results, together with the biophysical characterization reported above, suggested that **1** was a very encouraging hit compound able to compromise the catalytic activity of Ube2T, therefore suitable for further optimization.

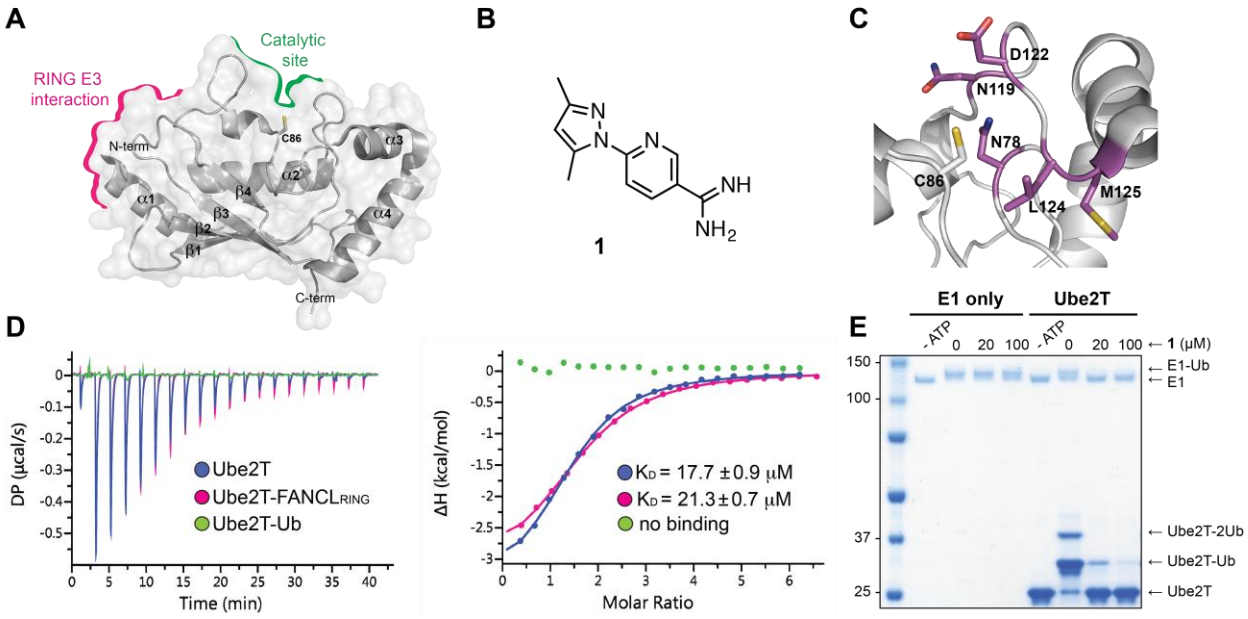

Figure 1. Biophysical and biochemical characterization of compound **1**. (**A**) Ube2T structure showing the typical E2 UBC fold. (**B**) Chemical structure of **1**. (**C**) **1** binding site determined by protein-observed NMR and mapped on Ube2T crystal structure. Residues colored in magenta correspond to ^{15}N-Ube2T HSQC resonances affected by the addition of **1** (see also Figure S2). (**D**) ITC titrations of 1.5 mM **1** against ~50 µM of the different Ube2T constructs indicated, details are reported in Table S1. (**E**) Representative coomassie stained gel of the biochemical assay monitoring the ubiquitin-charging of Ube2T in presence of compound **1**. The left lanes show a control reaction in which Ube2T is absent.

Synthesis of compound 1 analogues

In order to optimize the binding affinity of compound **1**, we set up crystallization experiments aimed to determine the mode of binding of **1**. In parallel, we designed a small library of compounds (**2**-**14**) to begin to evaluate structure activity relationships (Chart 1).

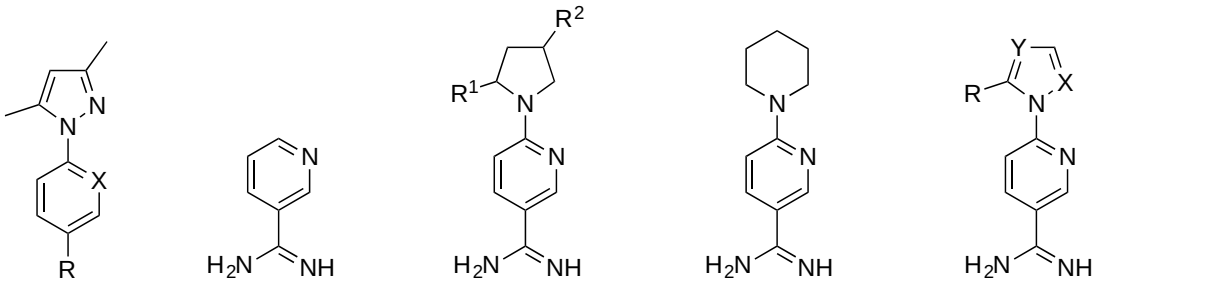

2: R = H, X =N
3: R = CO_2H, X = N
4: R = $CONH_2$, X = N
5: R = CH_2NH_2, X = N
6: R = SO_2NH_2, X = CH
7: R = $C(NH)NH_2$, X = CH

8

9: $R^1 = R^2 = H$
10: $R^1 = CH_3$, $R^2 = H$
11: $R^1 = H$, $R^2 = CH_3$

12

13: R = H, X = N, Y = CH
14: R = CH_3, X = CH, Y = N

Chart 1. Chemical structure of compound **1** analogues. Derivatives **1**, **2**, **3**, **5**, **6**, **8**, **9**, **12** were purchased from a commercial vendor. **4**, **7**, **10**, **11**, **13**, **14** were synthesized.

First, the amidine moiety was removed or replaced by a primary amine, an amide or a carboxylate (derivatives **2**-**6**). Compounds **2**, **3**, **5**, **6** and **7** were commercially available. Amide **4** was prepared from commercially available carboxylic acid **3** and ammonium chloride by HATU/*N,N*-diisopropylethylamine (DIPEA) mediated amide coupling. None of the compounds showed binding in ITC and DSF, suggesting that the amidine group is an essential feature for

binding. Different analogues were subsequently designed maintaining the amidine functionality intact and introducing modifications in the biaryl part of the molecule (Chart 1).

Non-commercially available amidines **10**-**11** were synthetized in house (Scheme 1) from 6-fluoronicotinonitrile **15** which was reacted with the appropriate pirrolidine and DIPEA in acetonitrile at 90 °C overnight, obtaining nitriles **16**-**17** in good yields after flash column chromatography purification. Nitriles **16**-**17** were treated with an excess of anhydrous gaseous hydrochloric acid in methanol to obtain imino ether hydrochlorides, which were treated with 7 M ammonia solution in methanol to obtain amidines **10**-**11** (50-65% yield after preparative HPLC).

Nitriles **18**-**20** were reacted with sodium methoxide in methanol at room temperature (Scheme 1) until full conversion to the corresponding imino ethers was observed by LC-MS. Reaction of the imidates (not isolated) with ammonium chloride afforded the expected amidines **7**, **13** and **14**, which were finally purified by HPLC.

Compounds **7**-**14** were tested in DSF and ITC, and surprisingly only derivatives **9** and **13** showed a concentration dependent effect in DSF (Figure S3). Only for compound **9** the K_D was measurable by ITC, although the affinity is much weaker (~ 500 μM). Compound **13** lacks the two methyl groups on the pyrazole ring, whereas **9** has a saturated pyrrolidine ring replacing the pyrazole. However, when the pyrrolidine moiety is 2- or 3- methyl substituted (derivatives **10** and **11**), or when it is replaced by a piperidine ring (compound **12**), binding is again completely abolished.

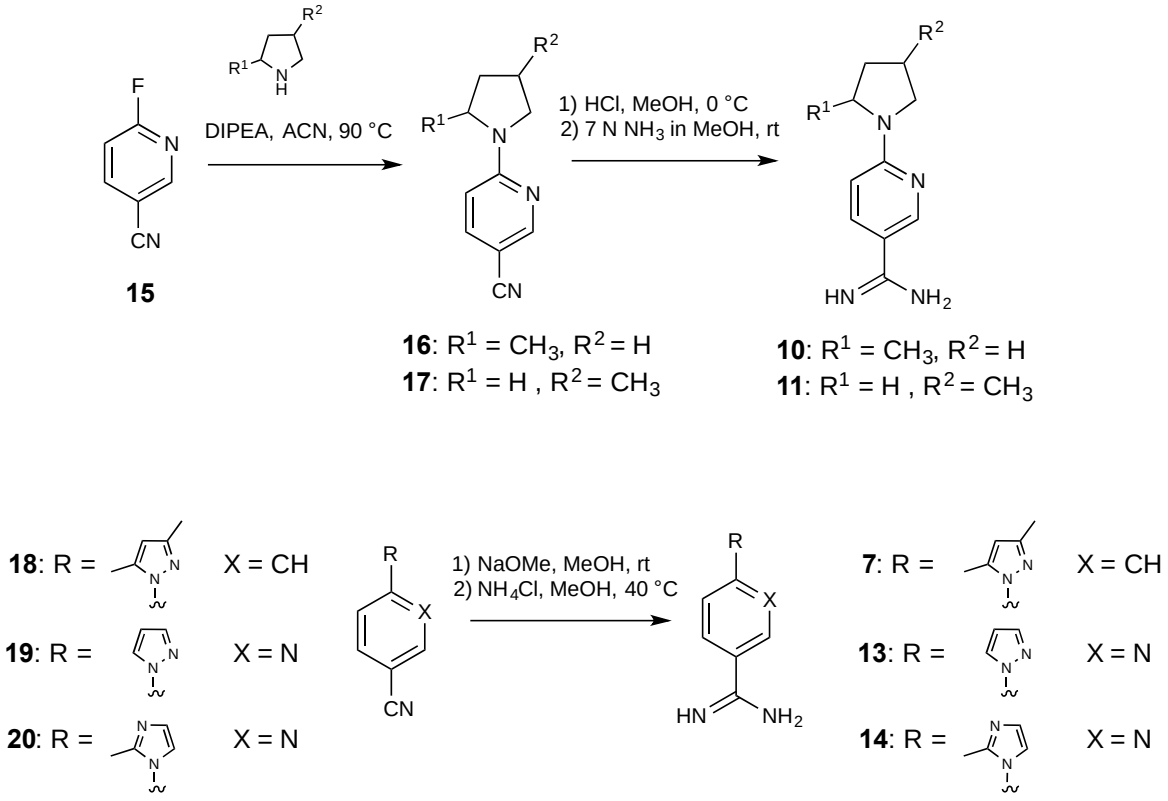

Scheme 1. Synthesis of amidines **7**, **10**, **11**, **13** and **14**.

Co-crystal structure reveals a metal mediated oligomer

The rather flat SAR results raised some concerns regarding compound **1**. Although quality control documents were provided by the commercial vendor, we repeated NMR and HRMS analyses, finding them in agreement with the declared structure (see Supplementary Information). Despite having identified the binding site by protein-observed NMR and confirmed it with solid binding data, yet the molecular details of compound **1** - Ube2T interaction were missing. Only a co-crystal structure could help in understanding why any minor change of the original compound **1** structure led to a complete loss in binding. For this reason, we pursued multiple co-crystallization attempts using different Ube2T constructs, including the full-length

protein (1-197), Ube2T$_{\Delta C}$ (1-154) and the Ube2T-FANCL$_{RING}$ fusion construct.[10] After many unsuccessful attempts, well-diffracting crystals of Ube2T$_{\Delta C}$ with compound **1** in a 1:5 molar ratio were eventually obtained. We solved the crystal structure at 1.85 Å (PDB ID: 5OJJ, Table S2) and discovered an unexpected arrangement of Ube2T molecules.

Contrary to all the other Ube2T structures in which Ube2T is monomeric (Figure 1A), our crystal structure contains six molecules in the asymmetric unit organized in two cyclic trimers (Figure 2). Each monomer has adopted an unusual conformation whereby the N-terminal α1-helix and β1-strand (first ~ 30 residues) have moved onto the nearby molecule of the trimer with a cyclic organization (chain A onto B, chain B onto C, chain C onto A, Figure 2A, B). This structural rearrangement is called 'domain swap': protein molecules exchange secondary structure elements to form an intertwined oligomer in which the overall fold of each monomer is maintained, with the exception of the hinge loop connecting the part that is exchanged.[15] In our structure the hinge loop is formed by residues Q26-D33. Interestingly, a domain swap of the same secondary structure elements has also been observed for a different E2, Ube2W (PDB entry 2A7L).[9] Ube2W however, forms a reciprocal dimer instead of a cyclic trimer (Figure S4).

Close analysis of the refined structure revealed that no organic molecule corresponding to compound **1** structure was bound to the protein at the catalytic site as suggested by the HSQC experiments, or anywhere else on the surface. However a strong and unexplained density, which suggested a metal ion, was connected to the catalytic cysteine (C86) (Figure S5 and S6). Given the coordination geometry and the nature of the chelating residues, we modeled a zinc ion. The tetrahedral coordination is completed by the S atom of C86, the ε amino group of K91, an acetate molecule from the crystallization buffer and by the π nitrogen of H150 from a different Ube2T

molecule (*Zinc site 1*, Figure 2B). This zinc chelation involving two different Ube2T monomers is responsible for the formation of the domain swapped cyclic trimer (Figure 2B, D).

Interestingly, when the trimer is formed, D127 residues from each Ube2T monomer come close together and chelate another Zn^{2+} ion through one oxygen atom of the carboxylate, further stabilizing the trimer assembly. At this second Zn^{2+} binding site (*Zinc site 2*, Figure 2C), the tetrahedral coordination is completed by the τ nitrogen of H12 from a different trimer, leading to an open ended linear assembly of trimers (Figure 2D, E).

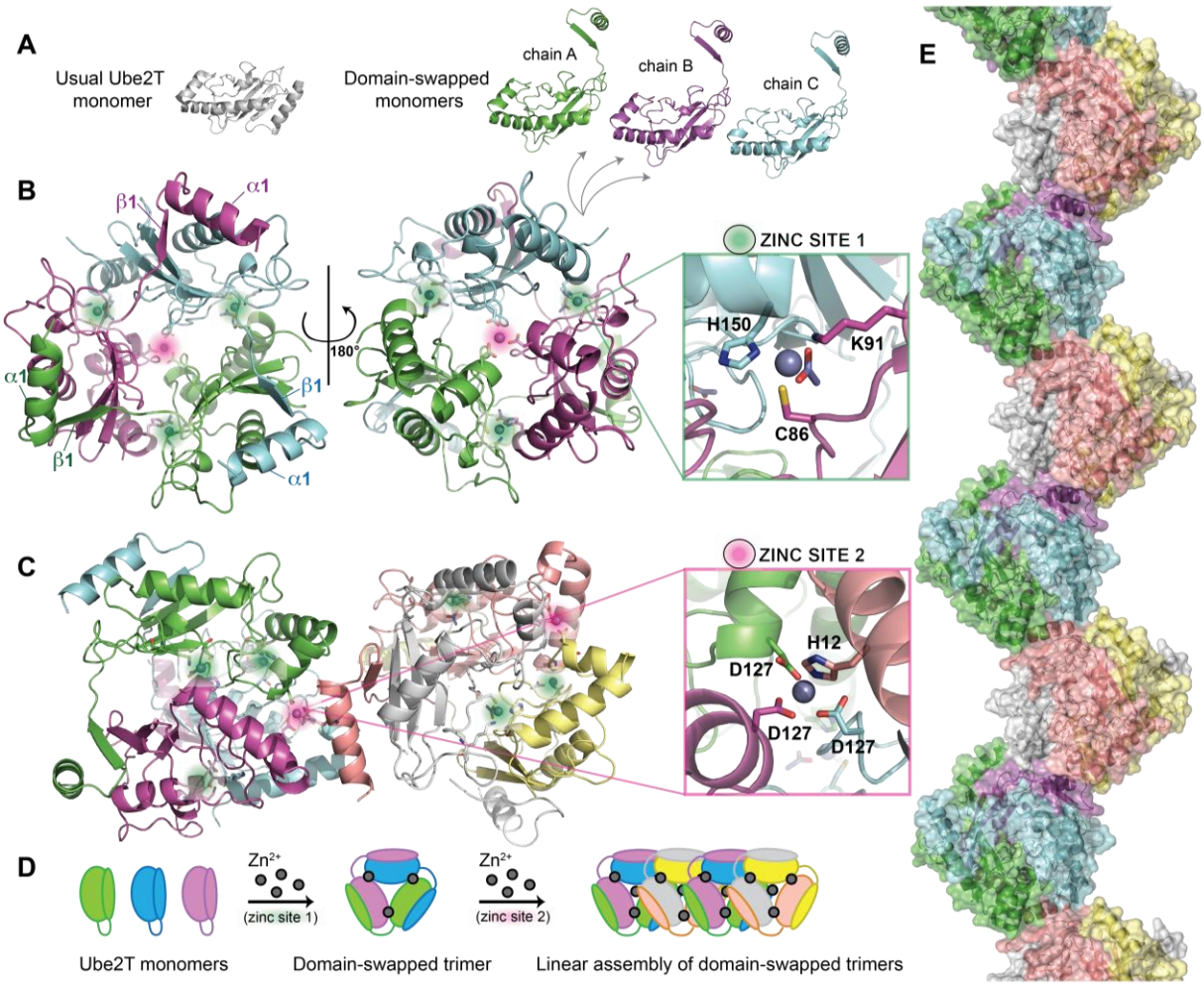

Figure 2. Zinc-mediated Ube2T$_{\Delta C}$ oligomerization. (**A**) Comparison between the usually observed Ube2T monomeric structure and the domain-swapped form. (**B**) Structure of the domain-swapped cyclic trimer held together by Zn^{2+} ions (PDB ID 5OJJ). The domain swap involves helix α1 and strand β1 of the three subunits. Each monomer binds a Zn^{2+} ion at the catalytic cysteine (*Zinc site 1*), connecting two monomers. (**C**) A second zinc binding site (*Zinc site 2*) is formed on the trimer by residues D127 of each of the three subunits, and is responsible for joining the trimers, with H12 from a different trimer completing the tetrahedral coordination. (**D**) Schematic representation of the zinc-induced domain swap and oligomerization. (**E**) Surface representation of the open-ended linear assembly of Ube2T$_{\Delta C}$ trimers.

Investigating zinc contamination in our compound series

In our structure, four zinc ions are bound to each Ube2T trimer, however no zinc salt is present in the crystallization buffer or is used during Ube2T expression and purification. Moreover, while performing co-crystallization trials, we noticed a direct correlation between compound **1** concentration and the number of crystals formed, with no crystallization occurring when **1** was absent. These observations led us to hypothesize that zinc may be present as a contaminant of the purchased compound **1** powder, and that the observed biophysical and biochemical effects of **1** could be attributed to the presence of zinc. To test this hypothesis we repeated the ITC experiments in presence of a chelating agent. Remarkably, no binding was observed in presence of 2 mM EDTA in the ITC buffer (Figure 3A), confirming that the exceptionally good activity of compound **1**, found during our fragment screening, is exclusively due to zinc contamination of the original powder.

Furthermore, when $ZnCl_2$ was titrated against Ube2T in ITC, the isotherm was almost identical to the one obtained for compound **1** (Figure 3A).

To further confirm the presence of zinc, we used a colorimetric reagent known as Zincon (2-carboxy-2'-hydroxy-5'-sulfoformazylbenzene), which has been used as a chromophore for the quantification of both zinc and copper ions in aqueous solution.[16] Zincon confirmed the presence of different amount of Zn^{2+} in compounds **1**, **9** and **13** (Figure 3B, **12** was used as negative control), proportional to their 'potency' in DSF and ITC, ultimately explaining the flat and curious SAR of this compound series.

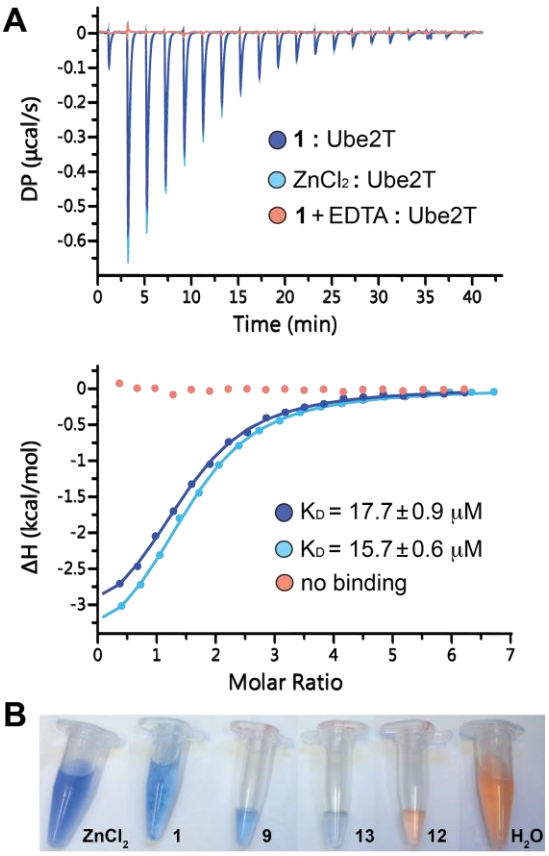

Figure 3. Confirmation of zinc contamination and binding effect. (**A**) The superposition of $ZnCl_2$ and **1** titration against Ube2T shows an almost identical profile. Binding is lost when **1** is titrated against Ube2T in presence of EDTA. (**B**) Zincon colorimetric assay performed on compounds **1**, **9**, **13** and **12** shows correlation between the amount of zinc present and the observed binding potency. Water and $ZnCl_2$ are used as references for the observed color changes.

SUMMARY AND CONCLUSIONS

False positives are known to permeate the initial pool of hits from many compound screenings. To mitigate this effect, multiple assays are often performed in parallel to identify genuine binders and exclude interferences related to a single detection method, effects that can arise from aggregation, or covalent and non-specific crosslinking. In this context, our compound **1** case was particularly challenging. We detected binding in DSF and BLI, where we observed a rather normal association and dissociation profile. We mapped the binding site through protein-observed NMR spectroscopy and we measured the binding affinity by ITC. Through ITC we were also able to estimate the stoichiometry of interaction, which appeared to be close to **1**, as one would expect from a genuine binder. Compound **1** binding resulted in inhibition of Ube2T enzymatic activity, as demonstrated using a biochemical assay. All these results obtained for compound **1** were concentration dependent and consistent, until the unusual SAR raised the first suspicions. At last, only the crystal structure could tell us what was the real 'active ingredient' of our powder, which was not detectable through routine LC-MS and NMR quality control.

Our story serves as a cautionary tale for screening small molecules libraries, in particular when trying to target ubiquitin-conjugating enzymes (or cysteine containing enzymes in general). Hermann et al. have also reported that zinc and other metal impurities, often derived from the synthetic procedures, may affect a number of targets or assays.[17] The effect of contaminating metals can be recognized by repeating certain assays in presence of chelating agents (such as EDTA), when this is compatible with the assay setup and the protein structure (e.g. chelating agents should be avoided when structural or catalytic metals are part of the protein of interest).

In our study, the unexpected structural arrangement induced by zinc opens up new prospects. Although the micromolar affinity of Zn towards Ube2T excludes a physiological relevance of this interaction, analysis of the zinc-induced oligomerization may provide an interesting model for designing metal mediated protein-protein interactions. Indeed, work from several research groups has been focused on controlling proteins self-assembly into polymeric architectures by designing metal binding sites,[18-21] which add strength directionality and selectivity to the interaction, as metal chelation geometries and preferences are well understood.[22]

Another important feature of our structure is the domain swap of the N-terminal α1-helix and β1-strand of Ube2T, which is also observed for a different E2, Ube2W.[9] Previous studies have indeed highlighted that the swaps adopted by members of a protein family are characteristic traits of the protein fold.[23, 24] Domain swap has been often associated with a high degree of structural plasticity, as an example, GB1 protein (immunoglobulin-binding domain B1 of streptococcal protein G) has been named 'protein contortionist' for its ability to form a swapped dimer, a tetramer, or an amyloid fibril upon mutation of specific residues.[25-27]

Although the biological role of protein domain swapping remains elusive, it has attracted much interest because of its potential involvement in protein misfolding and aggregation processes associated with amyloid formation and prion diseases.[28-30]

Different mechanisms have been proposed for the monomer to oligomer transition. These include formation of an 'open' intermediate, or a transition in which conformational changes of individual monomers and their association are tightly coupled to minimize solvent exposure.[24] Another hypothesis is the formation of an unfolded state prior to oligomer assembly. Irrespective of the domain swap, different changes in the environmental conditions (pH, temperature, salt ions) may destabilize the monomeric folded state of a protein and trigger aggregation.[31] In our

system, we observed significant destabilization of Ube2T in presence of zinc, with decrease of the protein unfolding temperature in DSF. We therefore hypothesize that zinc binding at the catalytic cysteine promotes the domain swap either by an allosteric mechanism or by inducing an intermediate unfolded state. The observed structural plasticity for Ube2T and Ube2W, together with the induced allosteric effect across the UBC fold proposed here for Ube2T, might emerge as a common characteristic for the ubiquitin-conjugating enzyme family.

EXPERIMENTAL SECTION

Protein Expression and purification

All the Ube2T constructs were expressed and purified as described previously.[4, 10] In order to generate a stable ubiquitin-loaded Ube2T, the catalytic cysteine was mutated to a lysine (C86K) and the two lysines close to the catalytic site were mutated to arginines (K91R and K95R). Ubiquitin was then enzymatically linked to K86 through an isopeptide bond between ubiquitin C-terminus and the ε amino group of K86, as described by Plechanovová et al.[32]

Fragment screening

Our fragment screening cascade consisted of a combination of biophysical methods. DSF, BLI and protein-observed NMR were performed as described previously.[4] However, for DSF and HSQC experiments, lower compound concentrations were used compared to the other fragments reported in our previous study.[4] For the DSF experiments, 40 µL samples were prepared in duplicates using 5 µM Ube2T, 2.5x SYPRO orange in 100 mM Tris pH 8.0, 100 mM NaCl, 0.25

mM TCEP and a compound concentration ranging from 5 μM to 5 mM. The samples were heated from 25 °C to 95 °C with increments of 1 °C/minute, and fluorescence was measured at each step. Data analysis was performed as described by Niesen et al.[33]

Nuclear Magnetic Resonance Spectroscopy

[^{1}H–^{15}N]-HSQC spectra were recorded on 50 μM ^{15}N-Ube2T$_{\Delta C}$ with increasing compound **1** concentration (100 μM, 300 μM and 500 μM) as described previously.[4] A superposition of the apo-protein spectrum with the spectrum recorded at the highest compound **1** concentration tested is shown in Figure S2. Compound **1** was then dialyzed out overnight in the same buffer used for the described NMR experiments (50 mM Potassium phosphate pH 6.8, 85 mM NaCl, 1 mM DTT). After dialysis a new HSQC spectrum was recorded, showing that the signals position in the apo Ube2T spectrum was restored.

Isothermal Titration Calorimetry

All the experiments were carried out using the MicroCal PEAQ-ITC (Malvern) and analyzed using the MicroCal PEAQ-ITC Analysis Software. All the titrations were performed at 25 °C, whilst stirring at 750 rpm in a buffer containing 100 mM Tris pH 8.0, 100 mM NaCl, 0.5 mM TCEP. A control experiment of titrant into buffer was performed in order to account for the heat of dilution. All the titrations were repeated at least twice with similar results. For all the titrations an approximate protein concentration of 50 μM was used. Detailed concentrations and thermodynamic parameters per each fitted ITC experiment are reported in Table S1.

Ube2T charging assay

Ube2T charging reactions (20 μl) contained 20 μM ubiquitin, 0.2 μM of recombinant human E1, 10 μM Ube2T and 5 mM ATP. Reactions were carried out for 10 minutes at 30 °C and terminated with non-reducing LDS loading buffer. The samples were resolved by SDS-PAGE and coomassie stained (Figure 1E). All the experiments were repeated at least twice with similar results.

Synthetic procedures

All chemicals, unless otherwise stated, were commercially available and used without further purification. Reactions were magnetically stirred; commercially available anhydrous solvents were used. Flash column chromatography (FCC) was performed using a Teledyne Isco Combiflash Rf or Rf200i, prepacked columns RediSep Rf Normal Phase Disposable Columns were used. NMR spectra were recorded on a Bruker Ascend 400. Chemical shifts are quoted in ppm and referenced to the residual solvent signals: ^{1}H δ = 7.26 ppm ($CDCl_3$), 4.79 ppm (D_2O), 2.50 ppm (DMSO-d_6), ^{13}C δ = 77.2 ppm ($CDCl_3$), 39.5 ppm (DMSO-d_6); signal splitting patterns are described as singlet (s), doublet (d), doublet of doublet (dd), triplet (t), quartet (q), multiplet (m), broad (br). Coupling constants ($J_{H–H}$) are measured in Hz. High resolution mass spectra (HRMS) were recorded on a Bruker microTOF. Low resolution MS and analytical HPLC traces were recorded on an Agilent Technologies 1200 series HPLC connected to an Agilent Technologies 6130 quadrupole LC–MS, connected to an Agilent diode array detector. Preparative HPLC was performed on a Gilson preparative HPLC system with a Waters X-Bridge C18 column (100 mm × 19 mm; 5 μm particle size). Elution conditions are reported in the general methods. The purity of all compounds was analyzed by HPLC–MS (ESI) and was >95%.

***6-(3,5-dimethyl-1H-pyrazol-1-yl)nicotinamide* (4).** To a solution of **3** (20 mg, 0.092 mmol) in DMF (4 mL), HATU (53 mg, 0.138 mmol), NH_4Cl (10 mg, 0.184 mmol) and DIPEA (63 µL, 0.368 mmol) were added. The reaction mixture was stirred at room temperature for 3 hours, the solvent was then removed under reduced pressure. The crude was dissolved in DCM (5 mL) and washed with water (2 mL) and the organic layer was dried over anhydrous $MgSO_4$. DCM was removed under reduced pressure and the crude was dissolved in methanol and purified by preparative HPLC (gradient of 5–95% acetonitrile in water with 0.1% formic acid over 10 min, flow 25 mL/min) and freeze-dried to obtain the title compound as a white powder, 12 mg, 60% yield. ^{1}H NMR (400 MHz, DMSO) δ: 8.86 (d, J=2.7 Hz, 1H), 8.31 (dd, J=2.5, 8.6 Hz, 1H), 7.86 (d, J=8.5 Hz, 1H), 6.15 (s, 1H), 2.59 (s, 3H), 2.19 (s, 3H). ^{13}C NMR (101 MHz, DMSO) δ: 166.3, 155.0, 150.2, 147.7, 141.9, 138.6, 127.1, 114.6, 110.3, 15.1, 13.9. HRMS m/z calcd for $C_{11}H_{12}N_4O$: 216.1011, found 217.1032 [M + H^+].

***4-(3,5-dimethyl-1H-pyrazol-1-yl)benzimidamide, formate salt* (7).** Prepared accordingly to general method A. 19 mg, 37% yield, white solid. ^{1}H NMR (400 MHz, D_2O) δ: 8.43 (s, 1H), 7.88 (d, *J*=8.6 Hz, 2H), 7.58 (d, *J*=8.9 Hz, 2H), 6.19 (s, 1H), 2.30 (s, 3H), 2.25 (s, 3H). ^{13}C NMR (101 MHz, D_2O) δ: 170.9, 165.8, 151.3, 143.2, 142.1, 129.0, 126.6, 124.6, 108.1, 12.1, 11.5. HRMS m/z calcd for $C_{12}H_{14}N_4$: 214.1218, found 215.1227 [M + H^+].

***6-(2-methylpyrrolidin-1-yl)nicotinimidamide* (10).** Prepared accordingly to general method B. 32 mg, 42 % yield, white solid. ^{1}H NMR (400 MHz, D_2O) δ: 8.40 (d, *J*=2.6 Hz, 1H), 8.11 (dd, *J*=2.1, 9.7 Hz, 1H), 7.28 - 7.15 (m, 1H), 4.39 (br. s, 1H), 3.83 - 3.76 (m, 1H), 3.58 (br. s, 1H), 2.32 - 2.14 (m, 3H), 1.96 - 1.90 (m, 1H), 1.29 (d, *J*=6.4 Hz, 3H). ^{13}C NMR (101 MHz, D_2O) δ: 165.7, 162.5, 139.3, 138.3, 114.0, 111.9, 57.0, 48.2, 31.8, 22.3, 17.2. HRMS m/z calcd for $C_{11}H_{16}N_4$: 204.1375, found 205.1359 [M + H^+].

6-(3-methylpyrrolidin-1-yl)nicotinimidamide **(11).** Prepared accordingly to general method B. 30 mg, 40% yield, white solid. ^{1}H NMR (400 MHz, D2O) δ: 8.36 (dd, *J*=0.6, 2.3 Hz, 1H), 8.06 (dd, *J*=2.4, 9.8 Hz, 1H), 7.09 (d, *J*=9.2 Hz, 1H), 3.79 (br. s, 2H), 3.67 - 3.59 (m, 1H), 3.22 (br. s, 1H), 2.56 - 2.48 (m, 1H), 2.30 - 2.22 (m, 1H), 1.81 - 1.72 (m, 1H), 1.12 (d, *J*=7.0 Hz, 3H). ^{13}C NMR (101 MHz, D_2O) δ: 162.6, 151.1, 139.1, 138.7, 113.5, 111.9, 55.4, 48.2, 32.9, 32.2, 16.4. HRMS m/z calcd for $C_{11}H_{16}N_4$: 204.1375, found 205.1367 [M + H^+].

6-(1H-pyrazol-1-yl)nicotinimidamide, formate salt **(13).** Prepared accordingly to general method A. 16 mg, 37% yield, white solid. ^{1}H NMR (400 MHz, D_2O) δ: 8.79 (d, *J*=2.0 Hz, 1H), 8.55 (d, *J*=3.1 Hz, 1H), 8.44 (s, 1H), 8.32 (dd, *J*=2.4, 8.7 Hz, 1H), 7.96 (d, *J*=9.1 Hz, 1H), 7.91 (d, *J*=1.6 Hz, 1H), 6.66 (t, *J*=2.1 Hz, 1H). ^{13}C NMR (101 MHz, D_2O) δ: 171.0, 164.0, 153.7, 147.9, 144.3, 139.5, 129.1, 122.4, 112.7, 109.5. HRMS m/z calcd for $C_9H_9N_5$: 187.0858, found 188.0921 [M + H^+].

6-(2-methyl-1H-imidazol-1-yl)nicotinimidamide, formate salt **(14).** Prepared accordingly to general method A. 22 mg, 45% yield, white solid. ^{1}H NMR (400 MHz, D_2O) δ: 8.98 (d, *J*=2.5 Hz, 1H), 8.48 (dd, *J*=2.5, 8.6 Hz, 1H), 7.84 (d, *J*=8.6 Hz, 1H), 7.62 (d, *J*=1.7 Hz, 1H), 7.20 (d, *J*=1.7 Hz, 1H), 2.62 (s, 3H). ^{13}C NMR (101 MHz, D_2O) δ: 171.0, 163.9, 152.6, 148.3, 146.2, 140.1, 125.0, 124.5, 120.5, 118.9, 13.3. HRMS m/z calcd for $C_{10}H_{11}N_5$: 201.1014, found 202.1049 [M + H^+].

6-(2-methylpyrrolidin-1-yl)nicotinonitrile **(16).** Prepared accordingly to general method C. 72 mg, 77% yield, white solid. ^{1}H NMR (400 MHz, $CDCl_3$) δ: 8.39 (dd, *J*=0.7, 2.3 Hz, 1H), 7.54 (dd, *J*=2.5, 9.0 Hz, 1H), 6.33 (d, *J*=9.0 Hz, 1H), 4.21 (br. s, 1H), 3.59 - 3.55 (m, 1H), 3.42 - 3.35 (m, 1H), 2.18 - 2.00 (m, 3H), 1.82 - 1.73 (m, 1H), 1.22 (d, *J*=6.4 Hz, 3H). ^{13}C NMR (101 MHz,

$CDCl_3$) δ: 157.3, 153.2, 139.0, 119.3, 106.3, 94.8, 53.6, 47.2, 32.7, 23.0, 18.9. MS m/z calcd for $C_{11}H_{13}N_3$: 187.1, found 188.1 [$M + H^+$].

6-(3-methylpyrrolidin-1-yl)nicotinonitrile **(17).** Prepared accordingly to general method C. 69 mg, 74% yield, white solid. ^{1}H NMR (400 MHz, $CDCl_3$) δ: 8.39 (dd, *J*=0.7, 2.3 Hz, 1H), 7.55 (dd, *J*=2.3, 8.9 Hz, 1H), 6.31 (dd, *J*=0.8, 9.0 Hz, 1H), 3.74 - 3.44 (m, 3H), 3.02 (br. s, 1H), 2.46 - 2.37 (m, 1H), 2.21 - 2.12 (m, 1H), 1.70 - 1.61 (m, 1H), 1.14 (d, *J*=6.5 Hz, 3H). ^{13}C NMR (101 MHz, $CDCl_3$) δ: 157.6, 153.1, 139.0, 119.2, 106.0, 95.0, 54.0, 46.8, 33.2, 17.9. MS m/z calcd for $C_{11}H_{13}N_3$: 187.1, found 188.1 [$M + H^+$].

General method A. To a mixture of nitrile (0.24 mmol) and methanol (0.5 mL) in a microwave vial equipped with rubber septum and magnetic stirrer, a solution of sodium methoxide 0.5 M in methanol (0.5 mL, 0.25 mmol) was added under nitrogen atmosphere. The mixture was stirred at room temperature overnight. LC-MS analysis showed complete conversion of the nitrile to the imino ether. Ammonium chloride (16 mg, 0.30 mmol) was added and the solution was stirred for 8 h at 40 ºC. Solvent was removed under reduced pressure and the resulting solid was dissolved in methanol, purified by preparative HPLC (gradient of 5–95% acetonitrile in water with 0.1% formic acid over 10 min, flow 25 mL/min) and freeze-dried.

General method B. A solution of nicotinonitrile **16** or **17** (0. 37 mmol) in methanol (4 mL) was treated with gaseous anhydrous hydrochloric acid for 15 minutes at 0 ºC and the reaction mixture was left at room temperature for 3 hours. Volatile components were removed by means of a nitrogen stream and the resulting solid was dried under vacuum. The white solid was dissolved in 2 mL of 7 N ammonia in methanol, transferred in a microwave vial, sealed and left at room temperature for 24 hours. The solvent was removed under reduced pressure and the

resulting solid was dissolved in methanol, purified by preparative HPLC (gradient of 5–70% acetonitrile in water with 0.1% ammonia over 10 min, flow 25 mL/min) and freeze-dried.

General method C. To a solution of 6-fluoronicotinonitrile (61 mg, 0.5 mmol) in acetonitrile (0.5 mL) in a microwave vial, the desired methylpyrrolidine (0.75 mmol) and DIPEA (261 µL, 1.5 mmol) were added. The tube was sealed and heated at 90 ºC overnight. The solvent and volatile components were removed under reduced pressure and the crude mixture was purified by FCC over silica using heptane/ethyl acetate (8:2) as eluent mixture.

Crystallization and structure determination

The co-crystals were obtained by sitting drop vapor diffusion using 19.5 mg/mL Ube2T$_{\Delta C}$ (residues 1-154) and 5 mM compound **1** in a buffer containing 0.1 M Tris pH 8.0, 0.1 M NaCl, 0.25 mM TCEP. This solution was mixed 1:1 (1.5 µL + 1.5 µL) with the crystallization buffer containing 10% PEG3350, 0.2 M calcium acetate, 0.1 M Tris pH 8.5 and equilibrated against 0.5 mL of reservoir solution at 20 °C. Crystals appeared within a few hours. Crystals were cryoprotected with a solution containing 20% PEG3350, 0.2 M magnesium acetate, 0.1 M Tris pH 8.5 and flash frozen in liquid nitrogen. Data were collected at Diamond Light Source (i04-1 beamline) at 0.9282 Å wavelength and processed using XDS,[34] POINTLESS[35] and AIMLESS[36] from the CCP4 program suite[37] to a resolution limit of 1.85 Å (Table S2). The structure was solved by molecular replacement using PDB entry 1YH2[9] as a search model in MOLREP[38]. The first 32 amino acids were then deleted and manually rebuilt in Coot[39] in order to account for the domain swap that was unambiguous at such resolution. The domain swapped monomer was used again as a search model in MOLREP[38] and further refined using Refmac5[40] and Coot[39]. The

quality of the model was checked using MolProbity.[41] Zinc binding sites were validated using CheckMyMetal.[42]

Zincon assay

Zincon reagent was prepared by dissolving 4.35 mg of Zincon (Na^+ salt) in 200 μL of NaOH 0.5 M and then diluting it to 5 mL with water. In order to assess zinc contamination we diluted this stock solution 1:40 in 50 mM CHES pH 9.0 (orange solution) and added the analyzed compound at a final concentration of 2.5 mM. A clear color change to a blue solution was appreciable for those compounds contaminated with zinc (Figure 3B).

ASSOCIATED CONTENT

Supporting information

The Supporting Information is available free of charge on the ACS Publications website

Supplementary figures and Tables (PDF)

Molecular formula strings (CSV)

Accession codes

Atomic coordinates can be accessed using PDB ID code 5OJJ. Authors will release the atomic coordinates and experimental data upon article publication.

AUTHOR INFORMATION

Corresponding Author

* For H.W.: phone, +441382384109; e-mail: h.walden@dundee.ac.uk.

* A.C.: e-mail, a.ciulli@dundee.ac.uk.

Notes

The authors declare no competing financial interest

ACKNOWLEDGMENTS

This work was supported by the Medical Research Council (MRC grant number MC_UU_12016/12); the EMBO Young Investigator Programme to H.W.; the European Research Council (ERC-2015-CoG-681582 ICLUb consolidator grant to H.W.; ERC-2012-StG-311460 DrugE3CRLs starting grant to A.C.); the UK Biotechnology and Biological Sciences Research Council (BBSRC BB/G023123/2 David Phillips Fellowship to A.C.); and the Wellcome Trust (strategic awards 100476/Z/12/Z for biophysics and drug discovery and 094090/Z/10/Z for structural biology and X-ray crystallography to BCDD). We thank the Diamond Light Source for beamtime (BAG proposal MX10071) and beamline support at beamline I04-1.

ABBREVIATIONS

Ube2T, Ubiquitin-conjugating enzyme E2 T; PAINS, pan-assay interference compounds; DSF, differential scanning fluorimetry; BLI, bio-layer interferometry; ITC, isothermal titration calorimetry; HATU, 1-[Bis(dimethylamino)methylene]-1H-1,2,3-triazolo[4,5-b]pyridinium 3-oxid hexafluorophosphate; DIPEA, *N,N*-diisopropylethylamine; TCEP, tris(2-carboxyethyl)phosphine; LDS, lithium dodecyl sulfate; SDS-PAGE, sodium dodecyl sulphate -

polyacrylamide gel electrophoresis; FCC, flash column chromatography; CHES, N-Cyclohexyl-2-aminoethanesulfonic acid.

REFERENCES

1. Thorne, N.; Auld, D. S.; Inglese, J. Apparent activity in high-throughput screening: origins of compound-dependent assay interference. *Curr. Opin. Chem. Biol.* **2010,** *14*, 315-324.

2. Baell, J.; Walters, M. A. Chemistry: Chemical con artists foil drug discovery. *Nature* **2014,** *513*, 481-483.

3. McGovern, S. L.; Helfand, B. T.; Feng, B.; Shoichet, B. K. A specific mechanism of nonspecific inhibition. *J. Med. Chem.* **2003,** *46*, 4265-4272.

4. Morreale, F. E.; Bortoluzzi, A.; Chaugule, V. K.; Arkinson, C.; Walden, H.; Ciulli, A. Allosteric targeting of the Fanconi anemia ubiquitin-conjugating enzyme Ube2T by fragment screening. *J. Med. Chem.* **2017,** *60*, 4093-4098.

5. Stewart, M. D.; Ritterhoff, T.; Klevit, R. E.; Brzovic, P. S. E2 enzymes: more than just middle men. *Cell Res.* **2016,** *26*, 423-440.

6. Alpi, A. F.; Chaugule, V.; Walden, H. Mechanism and disease association of E2-conjugating enzymes: lessons from UBE2T and UBE2L3. *Biochem. J.* **2016,** *473*, 3401-3419.

7. Metzger, M. B.; Pruneda, J. N.; Klevit, R. E.; Weissman, A. M. RING-type E3 ligases: master manipulators of E2 ubiquitin-conjugating enzymes and ubiquitination. *Biochim. Biophys. Acta* **2014,** *1843*, 47-60.

8. Morreale, F. E.; Walden, H. Types of ubiquitin ligases. *Cell* **2016,** *165*, 248-248 e241.

9. Sheng, Y.; Hong, J. H.; Doherty, R.; Srikumar, T.; Shloush, J.; Avvakumov, G. V.; Walker, J. R.; Xue, S.; Neculai, D.; Wan, J. W.; Kim, S. K.; Arrowsmith, C. H.; Raught, B.; Dhe-Paganon, S. A human ubiquitin conjugating enzyme (E2)-HECT E3 ligase structure-function screen. *Mol. Cell. Proteomics* **2012,** *11*, 329-341.

10. Hodson, C.; Purkiss, A.; Miles, J. A.; Walden, H. Structure of the human FANCL RING-Ube2T complex reveals determinants of cognate E3-E2 selection. *Structure* **2014,** *22*, 337-344.

11. Hodson, C.; Cole, A. R.; Lewis, L. P.; Miles, J. A.; Purkiss, A.; Walden, H. Structural analysis of human FANCL, the E3 ligase in the Fanconi anemia pathway. *J. Biol. Chem.* **2011,** *286*, 32628-32637.

12. Alpi, A. F.; Pace, P. E.; Babu, M. M.; Patel, K. J. Mechanistic insight into site-restricted monoubiquitination of FANCD2 by Ube2t, FANCL, and FANCI. *Mol. Cell* **2008,** *32*, 767-777.

13. Walden, H.; Deans, A. J. The Fanconi anemia DNA repair pathway: structural and functional insights into a complex disorder. *Annu. Rev. Biophys.* **2014,** *43*, 257-278.

14. Dai, R.; Geders, T. W.; Liu, F.; Park, S. W.; Schnappinger, D.; Aldrich, C. C.; Finzel, B. C. Fragment-based exploration of binding site flexibility in Mycobacterium tuberculosis BioA. *J. Med. Chem.* **2015,** *58*, 5208-5217.

15. Rousseau, F.; Schymkowitz, J. W.; Itzhaki, L. S. The unfolding story of three-dimensional domain swapping. *Structure* **2003,** *11*, 243-251.

16. Sabel, C. E.; Neureuther, J. M.; Siemann, S. A spectrophotometric method for the determination of zinc, copper, and cobalt ions in metalloproteins using Zincon. *Anal. Biochem.* **2010,** *397*, 218-226.

17. Hermann, J. C.; Chen, Y.; Wartchow, C.; Menke, J.; Gao, L.; Gleason, S. K.; Haynes, N. E.; Scott, N.; Petersen, A.; Gabriel, S.; Vu, B.; George, K. M.; Narayanan, A.; Li, S. H.; Qian, H.; Beatini, N.; Niu, L.; Gan, Q. F. Metal impurities cause false positives in high-throughput screening campaigns. *ACS Med. Chem. Lett.* **2013,** *4*, 197-200.

18. Salgado, E. N.; Ambroggio, X. I.; Brodin, J. D.; Lewis, R. A.; Kuhlman, B.; Tezcan, F. A. Metal templated design of protein interfaces. *Proc. Natl. Acad. Sci. U. S. A.* **2010,** *107*, 1827-1832.

19. Luo, Q.; Dong, Z.; Hou, C.; Liu, J. Protein-based supramolecular polymers: progress and prospect. *Chem. Commun. (Camb)* **2014,** *50*, 9997-10007.

20. Brodin, J. D.; Carr, J. R.; Sontz, P. A.; Tezcan, F. A. Exceptionally stable, redox-active supramolecular protein assemblies with emergent properties. *Proc. Natl. Acad. Sci. U. S. A.* **2014,** *111*, 2897-2902.

21. Bai, Y.; Luo, Q.; Zhang, W.; Miao, L.; Xu, J.; Li, H.; Liu, J. Highly ordered protein nanorings designed by accurate control of glutathione S-transferase self-assembly. *J. Am. Chem. Soc.* **2013,** *135*, 10966-10969.

22. Laitaoja, M.; Valjakka, J.; Janis, J. Zinc coordination spheres in protein structures. *Inorg. Chem.* **2013,** *52*, 10983-10991.

23. Mackinnon, S. S.; Malevanets, A.; Wodak, S. J. Intertwined associations in structures of homooligomeric proteins. *Structure* **2013,** *21*, 638-649.

24. Wodak, S. J.; Malevanets, A.; MacKinnon, S. S. The Landscape of Intertwined Associations in Homooligomeric Proteins. *Biophys. J.* **2015,** *109*, 1087-1100.

25. Byeon, I. J.; Louis, J. M.; Gronenborn, A. M. A protein contortionist: core mutations of GB1 that induce dimerization and domain swapping. *J. Mol. Biol.* **2003,** *333*, 141-152.

26. Byeon, I. J.; Louis, J. M.; Gronenborn, A. M. A captured folding intermediate involved in dimerization and domain-swapping of GB1. *J. Mol. Biol.* **2004,** *340*, 615-625.

27. Louis, J. M.; Byeon, I. J.; Baxa, U.; Gronenborn, A. M. The GB1 amyloid fibril: recruitment of the peripheral beta-strands of the domain swapped dimer into the polymeric interface. *J. Mol. Biol.* **2005,** *348*, 687-698.

28. Bennett, M. J.; Sawaya, M. R.; Eisenberg, D. Deposition diseases and 3D domain swapping. *Structure* **2006,** *14*, 811-824.

29. Knaus, K. J.; Morillas, M.; Swietnicki, W.; Malone, M.; Surewicz, W. K.; Yee, V. C. Crystal structure of the human prion protein reveals a mechanism for oligomerization. *Nat. Struct. Biol.* **2001,** *8*, 770-774.

30. Liu, Y.; Gotte, G.; Libonati, M.; Eisenberg, D. A domain-swapped RNase A dimer with implications for amyloid formation. *Nat. Struct. Biol.* **2001,** *8*, 211-214.

31. Herczenik, E.; Gebbink, M. F. Molecular and cellular aspects of protein misfolding and disease. *FASEB J.* **2008,** *22*, 2115-2133.

32. Plechanovova, A.; Jaffray, E. G.; Tatham, M. H.; Naismith, J. H.; Hay, R. T. Structure of a RING E3 ligase and ubiquitin-loaded E2 primed for catalysis. *Nature* **2012,** *489*, 115-120.

33. Niesen, F. H.; Berglund, H.; Vedadi, M. The use of differential scanning fluorimetry to detect ligand interactions that promote protein stability. *Nat. Protoc.* **2007,** *2*, 2212-2221.

34. Kabsch, W. Xds. *Acta Crystallogr. D Biol. Crystallogr.* **2010,** *66*, 125-132.

35. Evans, P. Scaling and assessment of data quality. *Acta Crystallogr. D Biol. Crystallogr.* **2006,** *62*, 72-82.

36. Evans, P. R.; Murshudov, G. N. How good are my data and what is the resolution? *Acta Crystallogr. D Biol. Crystallogr.* **2013,** *69*, 1204-1214.

37. Winn, M. D.; Ballard, C. C.; Cowtan, K. D.; Dodson, E. J.; Emsley, P.; Evans, P. R.; Keegan, R. M.; Krissinel, E. B.; Leslie, A. G.; McCoy, A.; McNicholas, S. J.; Murshudov, G. N.; Pannu, N. S.; Potterton, E. A.; Powell, H. R.; Read, R. J.; Vagin, A.; Wilson, K. S. Overview of the CCP4 suite and current developments. *Acta Crystallogr. D Biol. Crystallogr.* **2011,** *67,* 235-242.

38. Vagin, A.; Teplyakov, A. Molecular replacement with MOLREP. *Acta Crystallogr. D Biol. Crystallogr.* **2010,** *66*, 22-25.

39. Emsley, P.; Lohkamp, B.; Scott, W. G.; Cowtan, K. Features and development of Coot. *Acta Crystallogr. D Biol. Crystallogr.* **2010,** *66*, 486-501.

40. Murshudov, G. N.; Skubak, P.; Lebedev, A. A.; Pannu, N. S.; Steiner, R. A.; Nicholls, R. A.; Winn, M. D.; Long, F.; Vagin, A. A. REFMAC5 for the refinement of macromolecular crystal structures. *Acta Crystallogr. D Biol. Crystallogr.* **2011,** *67*, 355-367.

41. Chen, V. B.; Arendall, W. B., 3rd; Headd, J. J.; Keedy, D. A.; Immormino, R. M.; Kapral, G. J.; Murray, L. W.; Richardson, J. S.; Richardson, D. C. MolProbity: all-atom structure validation for macromolecular crystallography. *Acta Crystallogr. D Biol. Crystallogr.* **2010,** *66*, 12-21.

42. Zheng, H.; Cooper, D. R.; Porebski, P. J.; Shabalin, I. G.; Handing, K. B.; Minor, W. CheckMyMetal: a macromolecular metal-binding validation tool. *Acta Crystallogr. D Struct. Biol.* **2017,** *73*, 223-233.

Table of Contents graphic

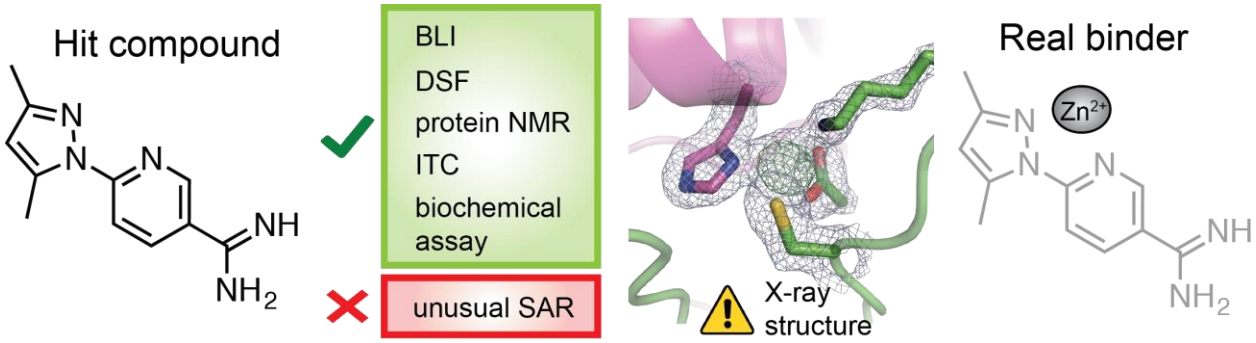

Supporting information

Mind the metal: a fragment library-derived zinc impurity binds the E2 ubiquitin-conjugating enzyme Ube2T and induces structural rearrangements

Francesca E. Morreale,[1] Andrea Testa,[2] Viduth K. Chaugule,[1] Alessio Bortoluzzi,[2] Alessio Ciulli,[2]* Helen Walden,[1]*

[1] MRC Protein Phosphorylation and Ubiquitylation Unit, School of Life Sciences, University of Dundee, Dundee DD1 5EH, United Kingdom

[2] Division of Biological Chemistry and Drug Discovery, School of Life Sciences, University of Dundee, Dundee DD1 5EH, United Kingdom

Table of Contents

SUPPLEMENTARY FIGURES AND TABLES

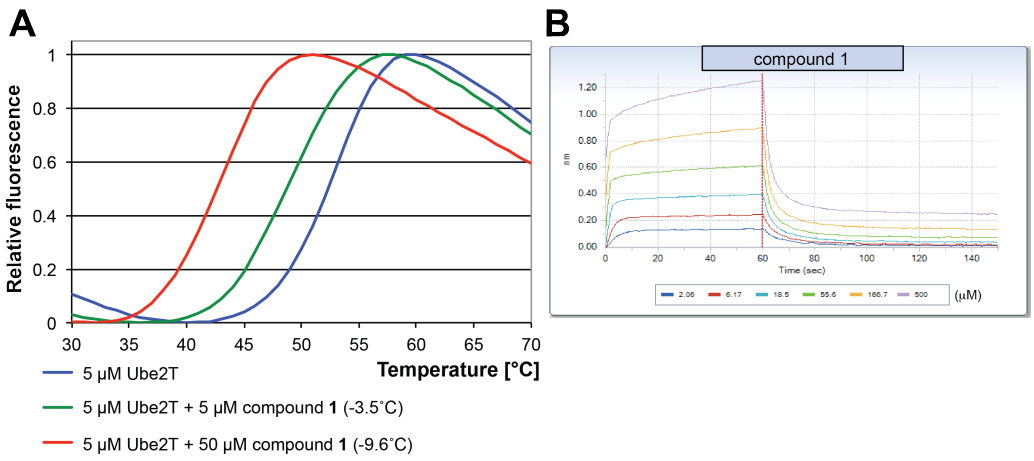

Figure S1. DSF (**A**) and BLI (**B**) results for compound **1**.

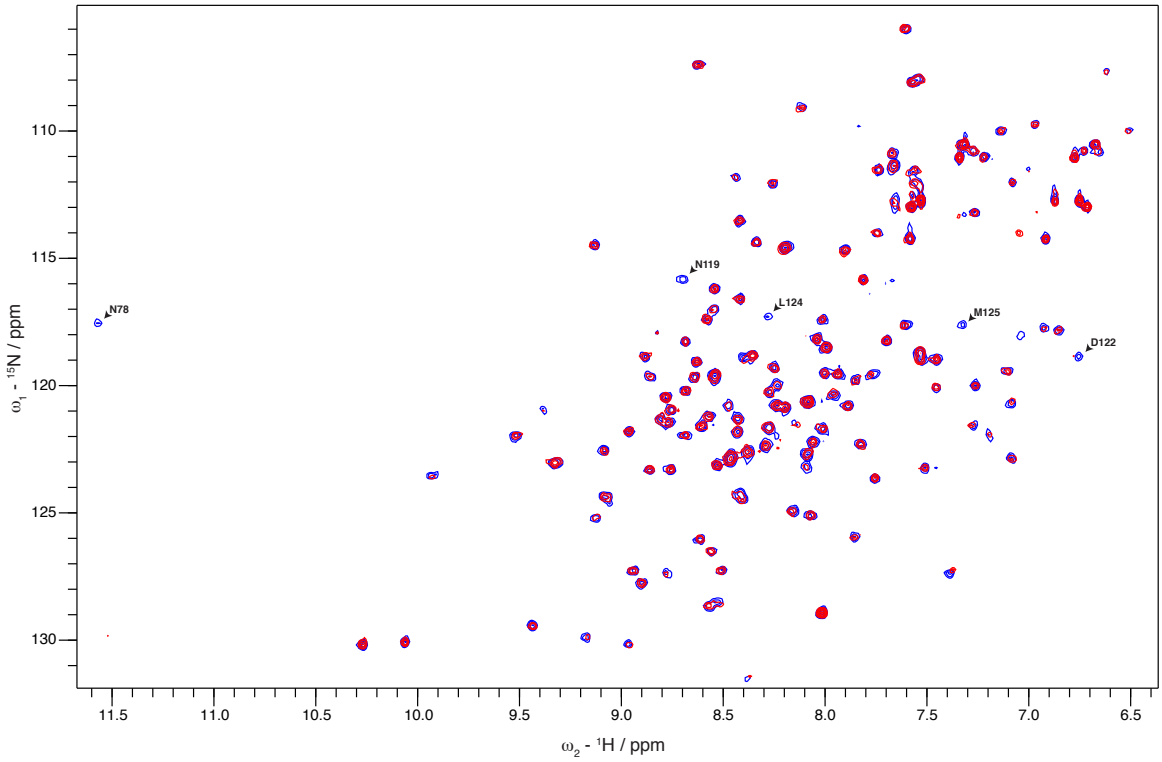

Figure S2. [^{15}N-^{1}H]-HSQC spectra recorded on 50 µM ^{15}N-Ube2T$_{\Delta C}$ (blue) and 50 µM ^{15}N-Ube2T$_{\Delta C}$ + 500 µM compound **1** (red).

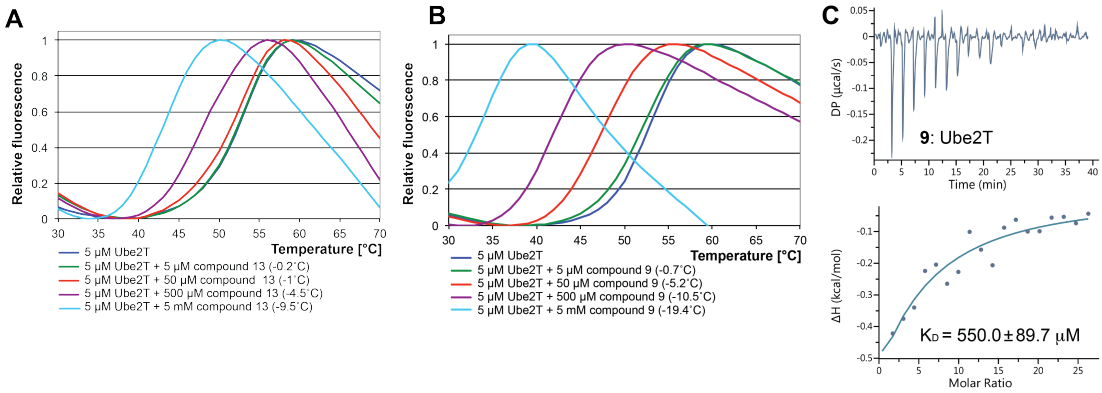

Figure S3. DSF results for compounds **13** (**A**) and **9** (**B**). (**C**) ITC titration of 5 mM **9** into 37.3 µM Ube2T.

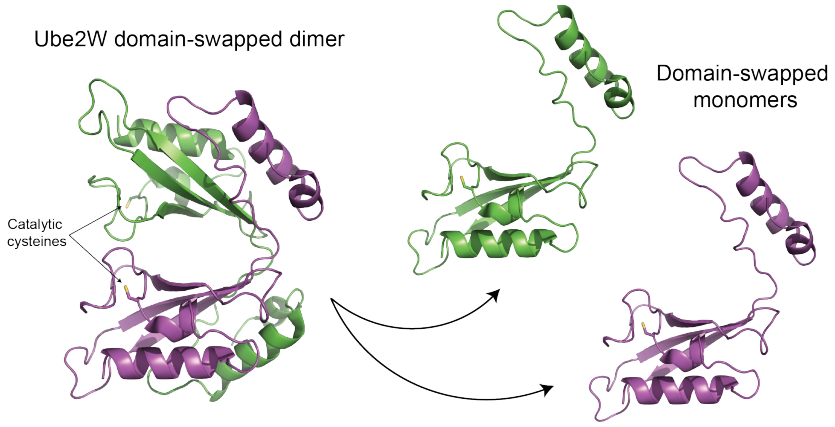

Figure S4. Ube2W domain-swapped crystal structure (PDB entry 2A7L, Sheng, Y. et al. *Mol. Cell. Proteomics* **2012,** *11*, 329-341).

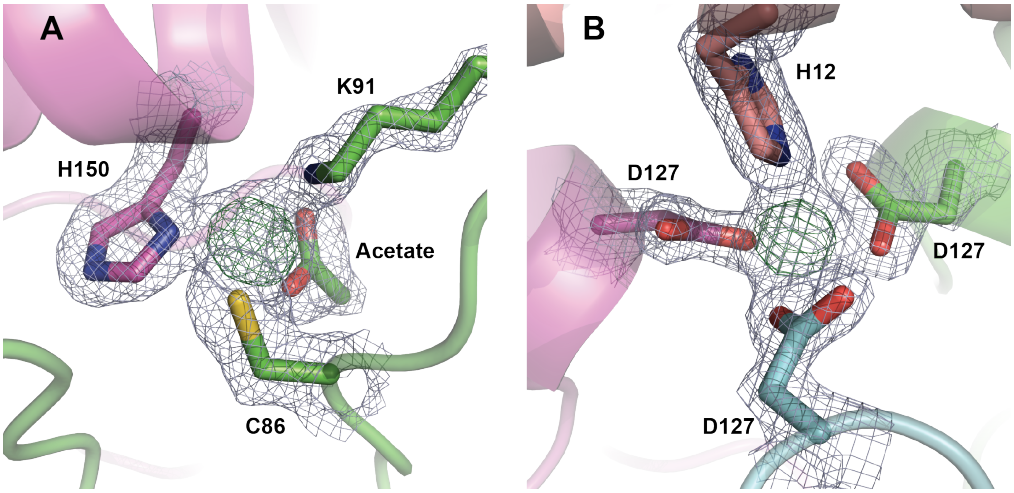

Figure S5. Electron density at the two zinc binding sites: (**A**) *Zinc site 1* and (**B**) *Zinc site 2*. In both panels show the electron density maps before fitting the Zn^{2+} ion. $2F_o$-F_c electron density map is contoured at 1.6σ level (grey) around the atoms shown in stick, and F_o-F_c electron density map is contoured at 15.0σ level (green).

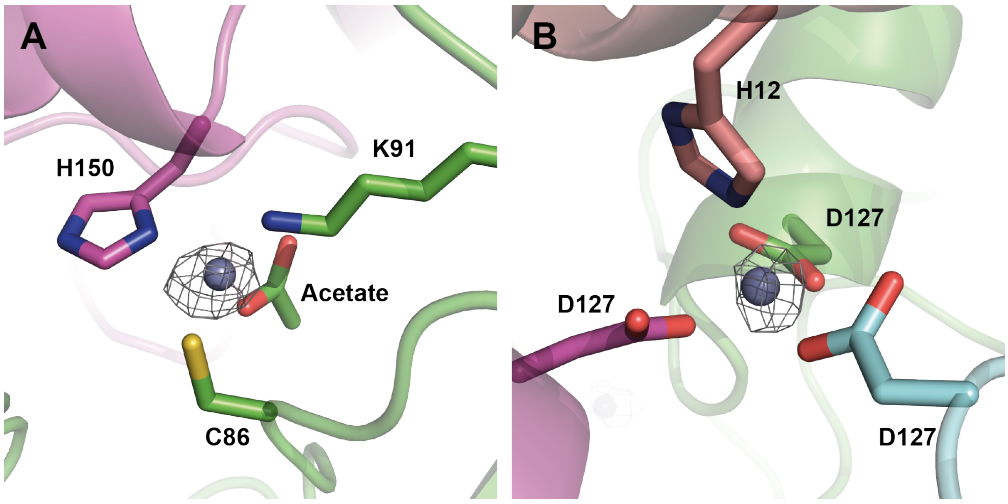

Figure S6. Anomalous difference electron density map at (**A**) *Zinc site 1* and (**B**) *Zinc site 2* contoured at 3σ.

Table S1. ITC data.

Syr:Cell	[Cell] (mM)	[Syr] (μM)	N (sites)	K_D (μM)	ΔH (kcal/mol)	ΔG (kcal/mol)	-TΔS (kcal/mol)
1:Ube2T	1.5	45.1	1.59 ± 0.02	17.7 ± 0.9	-3.60 ± 0.07	-6.49	-2.88
1:Ube2T-$FANCL_{RING}$	1.5	47.3	1.63 ± 0.02	21.3 ± 0.7	-3.31 ± 0.04	-6.37	-3.06
$ZnCl_2$:Ube2T	1.5	46.3	1.49 ± 0.02	15.7 ± 0.6	-3.93 ± 0.06	-6.55	-2.62
9:Ube2T	5	37.3	fixed to 1	550.0 ± 89.7	-7.69 ± 0.77	-4.45	3.24

Table S2. Data Collection and refinement statistics (PDB ID: 5OJJ).

Space group	$P12_11$
Molecules/ASU	6
Cell dimensions	
a, *b*, *c* (Å)	56.02, 96.38, 90.00
α, β, γ (°)	90.00, 93.28, 90.00
Resolution (Å)	48.75 – 1.85 (1.89 – 1.85)
Total reflections	276408 (13817)
Unique reflections	81137 (4465)
R_{merge}	0.038 (0.292)
$I/\sigma(I)$	16.6 (3.1)
$CC_{1/2}$	0.998 (0.849)
Completeness (%)	99.7 (99.6)
Redundancy	3.4 (3.1)
R_{work} / R_{free}	0.178/0.199
No. atoms	8268
Protein	7242
Water	978
Other hetero groups	48
Average *B* factor	29.0
R.m.s. deviations	
Bond lengths (Å)	0.011
Bond angles (°)	1.474
Ramachandran plot	
Favored (%)	97.53
Allowed (%)	2.47
Outliers (%)	0.0

Values in parentheses are for the highest resolution shell.

NMR spectra of compound **1** as received from commercial source.

^{1}H-NMR (400 MHz), D_2O

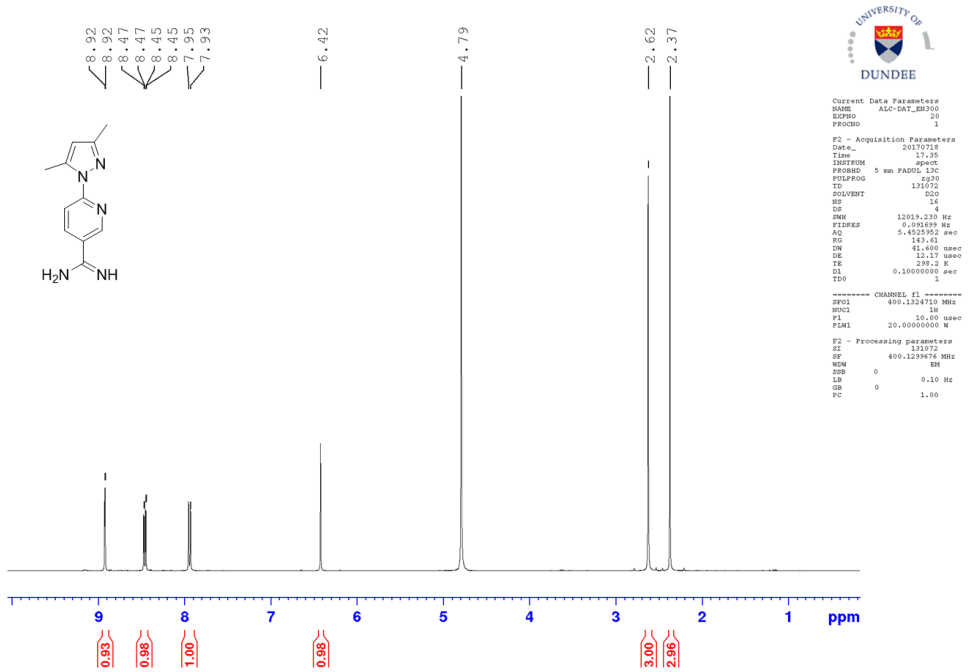

^{13}C-NMR (101 MHz), D_2O

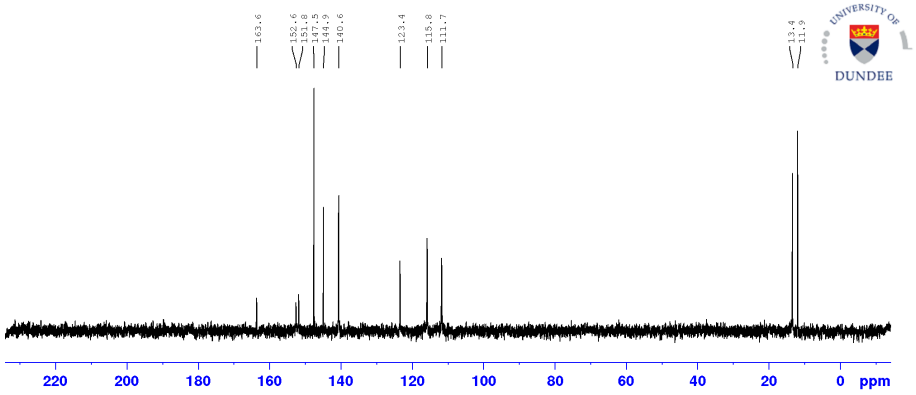

HSQC, D_2O

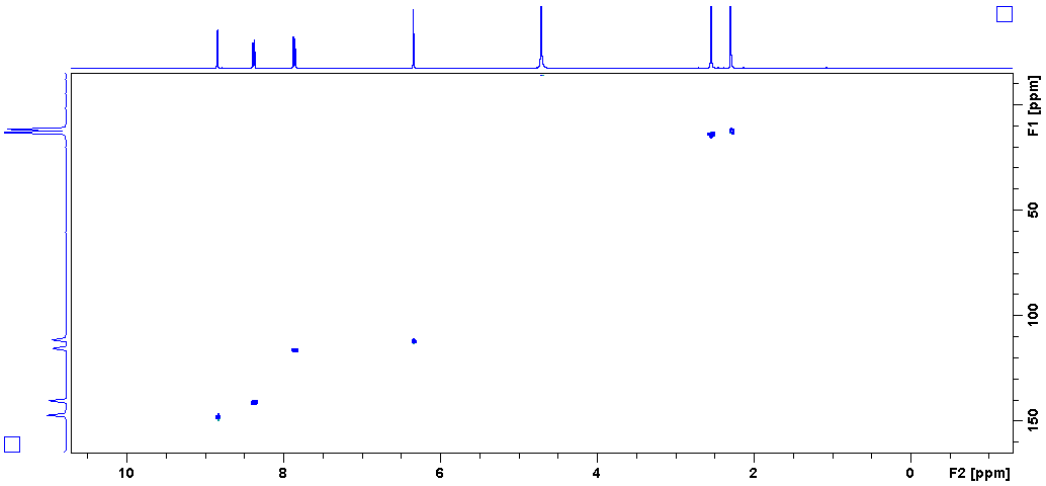

HRMS data for compound **1** as received from commercial source.

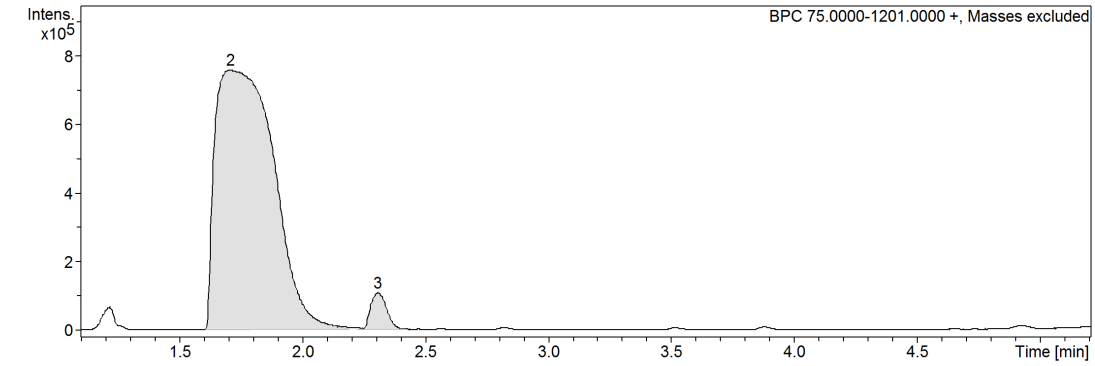

Sample Description

Method 1-microtof-2 Identify Compounds LCMS Pos 5-95.m

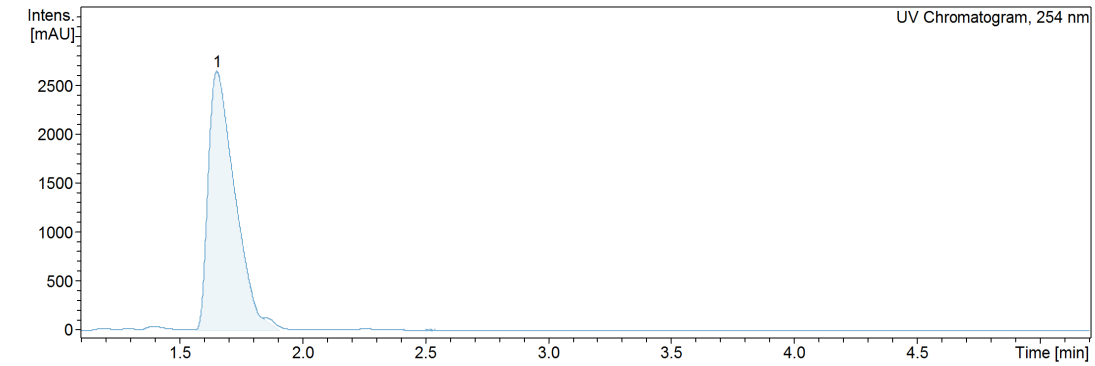

#	RT [min]	Area Frac. %	Chromatogram
1	1.7	100.00	UV Chromatogram, 254 nm
2	1.7	96.25	BPC 75.0000-1201.0000 +, Masses excluded
3	2.3	3.75	BPC 75.0000-1201.0000 +, Masses excluded

Cmpd 1, 1.7 min

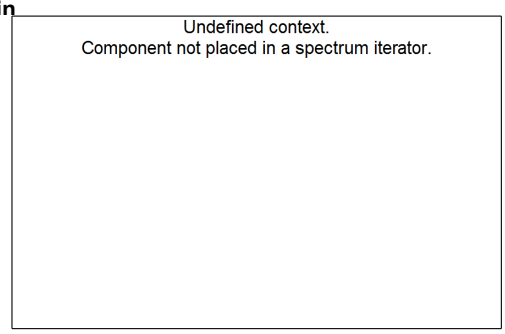

Cmpd 2, 1.7 min

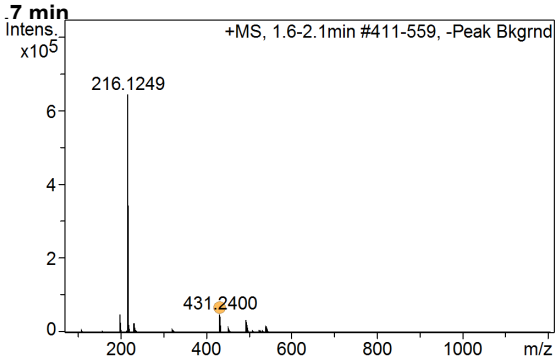

Cmpd 3, 2.3 min